

# Spirologozymes for Transesterifications: Design and Relationship of Structure to Activity

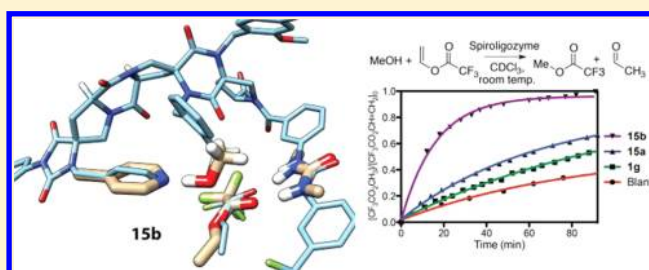
Mahboubeh Kheirabadi,<sup>†</sup> Nihan Çelebi-Ölçüm,<sup>‡</sup> Matthew F. L. Parker,<sup>†</sup> Qingquan Zhao,<sup>†</sup> Gert Kiss,<sup>‡</sup> K. N. Houk,<sup>\*,‡</sup> and Christian E. Schafmeister<sup>\*,†</sup>

<sup>†</sup>Department of Chemistry, Temple University, 1901 North 13th Street, Philadelphia, Pennsylvania 19122, United States

<sup>‡</sup>Department of Chemistry and Biochemistry, University of California at Los Angeles, Los Angeles, California 90095-1569, United States

## S Supporting Information

**ABSTRACT:** Transesterification catalysts based on stereochemically defined, modular, functionalized ladder-molecules (named spirologozymes) were designed, using the “inside-out” design strategy, and mutated synthetically to improve catalysis. A series of stereochemically and regiochemically diverse bifunctional spirologozymes were first synthesized to identify the best arrangement of a pyridine as a general base catalyst and an alcohol nucleophile to accelerate attack on vinyl trifluoroacetate as an electrophile. The best bifunctional spirologozyme reacted with vinyl trifluoroacetate to form an acyl-spirologozyme conjugate  $2.7 \times 10^3$ -fold faster than the background reaction with a benzyl alcohol. Two trifunctional spirologozymes were then synthesized that combined a urea with the pyridine and alcohol to act as an oxyanion hole and activate the bound acyl-spirologozyme intermediate to enable acyl-transfer to methanol. The best trifunctional spirologozyme carries out multiple turnovers and acts as a transesterification catalyst with  $k_1/k_{\text{uncat}}$  of  $2.2 \times 10^3$  and  $k_2/k_{\text{uncat}}$  of  $1.3 \times 10^2$ . Quantum mechanical calculations identified the four transition states of the catalytic cycle and provided a detailed view of every stage of the transesterification reaction.



## INTRODUCTION

Natural enzymes are proficient catalysts.<sup>1,2</sup> In the past few years, chemists have tried to mimic enzymes and to synthesize specially designed organocatalysts to optimize efficiency of many different transformations.<sup>3–10</sup> Despite many attempts to make such catalysts, the rational design of enzyme mimics is largely an unrealized dream.

Recently, we have developed the synthesis of highly functionalized and shape programmable macromolecules formed by coupling cyclic, stereochemically pure building blocks through pairs of amide bonds.<sup>11,12</sup> These molecules form spiro-fused oligomers (named spirologomers or bis-peptides) upon which functional groups can be displayed in controlled three-dimensional arrangements (Figure 1). We recently demonstrated a simple example of this strategy where the spiro linkage was used to place a phenyl group to stabilize the transition state of an aldol reaction by the hydrophobic effect.<sup>13</sup> Inspired by the success of the “inside-out” approach for the design of artificial enzymes<sup>14–16</sup> we have sought to apply this approach to the construction of catalytic spirologomers. This involves designing spirologomer scaffolds with fused-ring structures and stereochemical configurations that are capable of presenting catalytic functional groups in three-dimensional (3D) constellations suggested by theozyme calculations (Figure 1). To test our ability to design and synthesize more complex catalytic spirologomers using the “inside-out” design, we set out

to synthesize multifunctional spirologomers that could carry out a transesterification reaction. We call this class of spirologomer catalysts the “spirologozymes”, for short.

Esterases and proteases are enzymes that catalyze the hydrolysis of carboxyl esters and amides. Their high proficiency in hydrolysis is attributable to the high-level structural and electrostatic preorganization in their active sites.<sup>17–19</sup> They efficiently catalyze multiple chemical steps with minimal structural reorganization of the catalytic functionalities while maintaining optimal transition-state stabilization for each step during catalysis.<sup>17,19</sup> Recently, Houk and co-workers have used explicit solvent, periodic boundary molecular dynamics simulations to show that a naturally evolved cysteine protease cathepsin K has a well-defined active site with tightly maintained hydrogen bonds for the catalytic Cys-His-Asn triad in the dynamic environment.<sup>20</sup> The catalytic triad of Ser-His-Asp, originally described in chymotrypsin, is a classic structural motif in enzymology.<sup>21</sup> It was originally postulated that the catalytic triad enhances nucleophilicity of the hydroxyl group in the seryl residue to attack the acylating agents. Enhanced electron density on the serine hydroxyl necessitates deprotonation of the hydroxyl by His as a general base and neutralization of the generated charge being formed on the

Received: July 19, 2012

Published: September 19, 2012

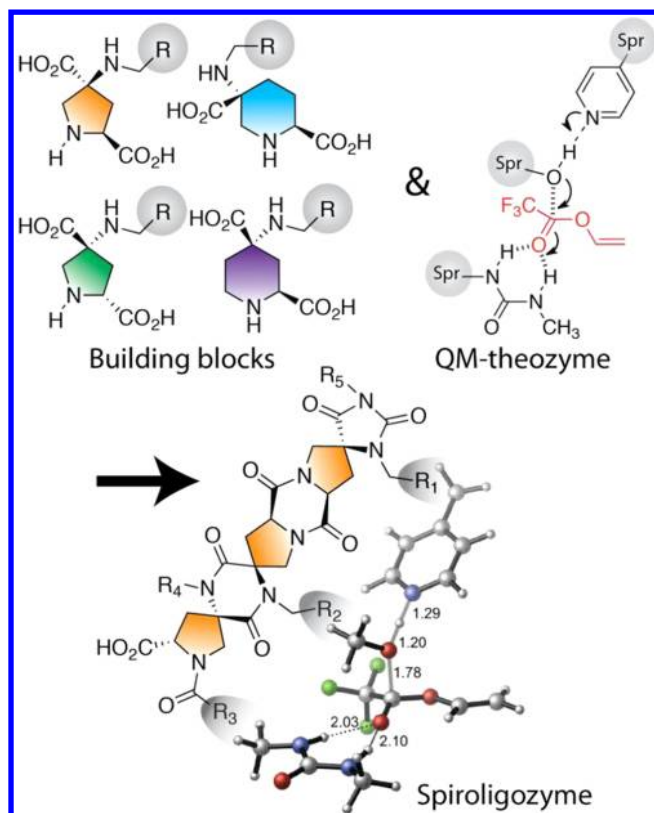


**Figure 1.** “Inside-out” approach to catalytic spirologomers. The program CANDO<sup>23</sup> is used to predict and design a spirologomer formed from the four building blocks to complement the nucleophilic transition state “theozyme” shown on the right.

imidazole moiety by another acid catalyzed interaction of His-Asp or His-Glu in the so-called “charge relay system”.<sup>21</sup> Subsequent discovery of similar triads in the subtilisin protease revealed that a specific oxyanion hole in the active site stabilizes the negative charge being formed on the substrate ester carbonyl oxygen in the tetrahedral intermediate.<sup>22</sup>

Recently, Baker and Houk have generated four artificial enzymes for ester hydrolysis by building nucleophilic dyads and oxyanion holes into protein scaffolds using the “inside-out” enzyme design strategy.<sup>24</sup> The most active of the variants catalyzed the cleavage of a *p*-nitrophenyl ester with a catalytic efficiency ( $k_{\text{cat}}/K_{\text{m}}$ ) of  $400 \text{ M}^{-1} \text{ s}^{-1}$  and a rate acceleration of approximately  $3.7 \times 10^3$ -fold over the background. Kinetic experiments showed that the protein is rapidly acylated as programmed by the design, but the subsequent deacylation step is slow and limits the overall catalytic efficiency.

A great deal of work has been carried out by chemists that demonstrates that converting intermolecular general acid/base reactions to intramolecular reactions on small organic scaffolds can enhance reaction rates by several orders of magnitude.<sup>17</sup> These model systems convert intermolecular general acid/base-catalyzed reactions to small (5–8 membered) ring hydrogen-bonded transition states that greatly enhance reaction rates by creating enormous effective molarities of the general acid/base in the reaction. Sakai and co-workers demonstrated a trifunctional small-molecule catalyst displaying a pyridine, an alcohol, and a urea that accelerates a transesterification reaction between vinyl trifluoroacetate and methanol by an impressive  $3.2 \times 10^4$ -fold for  $k_1/k_{\text{uncat}}$  and  $3.8 \times 10^3$ -fold for  $k_2/k_{\text{uncat}}$ .<sup>10</sup> Miller and co-workers screened small peptide libraries and

identified peptides that carry out enantioselective acyl transfer reactions.<sup>9,25</sup> Inspired by these results we sought to design transesterification catalysts by systematically incorporating and organizing increasing numbers of functional groups arranged on a modular spirologomer backbone in a way that would allow us to perturb the structures of the catalysts and observe the relationship between their structures and their catalytic rates.

## EXPERIMENTAL SECTION

**Theozyme Calculations.** Calculations were performed with *Gaussian 09*.<sup>26</sup> Transition states were located for the nucleophilic activation of vinyl trifluoroacetate in the presence of catalytic side chain mimics of enzymes and spirologozymes. Methanol, 4-methylimidazole, and acetate were used to mimic the nucleophilic triad of serine hydrolases and proteases, serine, histidine, and aspartate/glutamate, respectively. The nucleophilic dyad of spirologozymes was represented by methanol and 3- or 4-methylpyridine, depending on the attachment position of the pyridine to the spirologzyme backbone. Geometry optimizations were carried out at the B3LYP/6-31G(d) level of theory.<sup>27–30</sup> Solvent and medium effects were taken into account in the optimizations using the integral-equation-formalism polarizable continuum model (IEF-PCM).<sup>31–33</sup> A dielectric constant of 4 was used to represent the electrostatic environment of an enzyme active site for **TS1-triad**, and a dielectric continuum representing chloroform ( $\epsilon = 4.7$ ) was employed to solvate the spirologzyme model **TS1-dyad**. Energies were refined by single-point calculations with the M06-2X/6-31++G(2d,p)<sup>34</sup> using IEF-PCM with radii and nonelectrostatic terms for the SMD solvation model<sup>35</sup> as implemented in *Gaussian 09*.<sup>26</sup> Single-point energies in solution including all computed corrections were augmented with the correction to Gibbs free energy from unscaled B3LYP frequencies computed for 1 mol/L solute at 298 K. The free energies are reported in the text with respect to the separated substrate and preorganized catalyst complex.

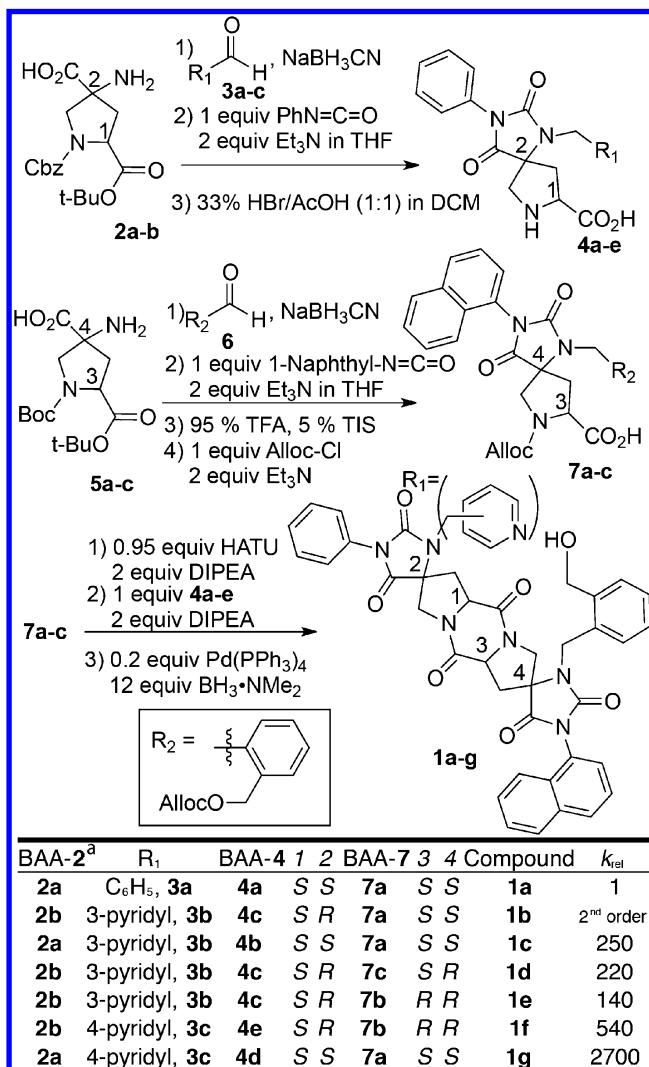
**Molecular Dynamics Simulations.** Molecular dynamics (MD) simulations were performed with *AMBER 11*<sup>36</sup> to evaluate whether the designed catalytic contacts were maintained in a dynamic environment in the presence of explicit solvent molecules. A recently described MD protocol for the evaluation of designed enzymes was employed.<sup>20</sup> This protocol predicted successfully the active and inactive designs for a set of Kemp elimination designs on the basis of the stability of the designed active sites. The spirologzyme parameters were generated with the antechamber module of *AMBER 11*<sup>36</sup> using the general *AMBER* force field (GAFF),<sup>37</sup> with partial charges set to fit the electrostatic potential generated at HF/6-31G(d) by RESP.<sup>38,39</sup> The charges were calculated according to the Merz–Singh–Kollman scheme<sup>40,41</sup> using *Gaussian 03*.<sup>26</sup> The spirologzymes were immersed in a chloroform box<sup>42</sup> ensuring a solvent layer of at least 10 Å around the spirologzymes. This resulted in the addition of up to 244 solvent molecules. A two-stage minimization approach was used. Initially, the positions of solvent molecules were minimized followed by an unrestrained minimization of all atoms. The systems were then heated in six 50 K, 50 ps steps from 0 to 300 K at constant volume periodic boundary conditions. Harmonic restraints of 10 kcal/mol were applied to the spirologzyme, and the Langevin equilibration scheme was used to control and equalize the temperature. A 1 fs time step was used during the heating stages to allow potential inhomogeneities to self-adjust. Each system was then equilibrated initially for 2 ns with a 2 fs time step at constant volume, followed by a 2 ns equilibration with a 2 fs time step at a constant pressure of 1 atm. A 20 ns production molecular dynamics simulation was carried out for each system using *PMEMD*<sup>43</sup> using the isothermal–isobaric ensemble (NPT). Long-range electrostatic effects were modeled using the particle-mesh-Ewald method.<sup>44</sup> Trajectories were saved every 100 steps (0.2 ps). This resulted in a total of 100,000 frames from the production MD run. Post-MD data analysis was performed using the ptraj module of *AMBER 11*.<sup>36</sup> In order to investigate the effect solvent on the preorganization of the catalytic functional groups, simulations were also carried out in a box of dichloromethane molecules.<sup>45</sup>

**Conformational Analysis.** An extensive conformational search was carried out for each designed spiroligozyme using *Macromodel*<sup>46</sup> to explore their structural preferences. The conformational search was carried out with the OPLS-2005 force field<sup>47</sup> using a mixed torsional and low mode sampling procedure as implemented in *Macromodel*. Polak–Ribiere Conjugate Gradient minimization method<sup>48</sup> was used with convergence criterion for energy set to <0.001 kJ/mol. The solvent effects were taken into account using the GB/SA solution model,<sup>49</sup> which treats the solvents as a fully equilibrated analytical continuum starting near the van der Waals surface of the solute, with parameters for chloroform. The conformational search produced 1557 conformers in the range of 5 kcal/mol. The resulting structures were clustered, and a total of 25 lowest-energy conformers were selected for further optimization using density functional theory. In order to provide an extended sampling and a more complete representation of the conformational space, a set of 20 representative snapshots was also selected from the 20 ns MD production run for additional analysis with density functional theory. OPLS-2005 and GAFF are specifically parametrized for the accurate treatment of small organic molecules.<sup>37,47</sup> The selected 45 structures were subjected to full geometry optimization with M06-2X/6-31G(d)<sup>34</sup> in a dielectric continuum treated with IEF-PCM solvation model<sup>31–33</sup> representing chloroform as the solvent. Single-point energies including radii and non-electrostatic terms for the SMD solvation model<sup>35</sup> were calculated at the same level of theory. All 45 conformers for each spiroligozyme were sorted with respect to their energies in solution including all computed corrections. All density functional theory calculations were performed using *Gaussian 09*.<sup>26</sup>

**Calculation of the Energy Profile.** All stationary points for the spiroligozyme-catalyzed acyl transfer reaction from vinyl trifluoroacetate to methanol were located using *Gaussian 09*.<sup>26</sup> ONIOM MO:MO type calculations<sup>50–52</sup> were used for the geometry optimizations, as high-accuracy model chemistries scale unfavorably with the size of the molecule. Two layers were defined within the structure, and they were treated at different levels of theory. The high level was composed of 4-methylpyridine, *o*-tolylmethanol, 1-(3,5-bis(trifluoromethyl)phenyl)-3-phenylurea groups of the spiroligozyme and the substrates (vinyl trifluoroacetate and methanol) and was treated with density functional B3LYP/6-31G(d).<sup>27–30</sup> The low level included the atoms of the spiroligozyme backbone and was treated at the semiempirical PM6 level of theory.<sup>53</sup> The transition states were characterized using the harmonic vibrational frequencies. Due to a convergence failure in the ONIOM optimization of TS3, this transition state was located using a relaxed potential energy surface scan for the formation of the C–O bond with 0.01 Å increments between  $d_{(C-O)} = 1.93$  Å and  $d_{(C-O)} = 1.71$  Å (see the SI). The energies of all located stationary points were refined with single-point calculations on the complete system at the M06-2X/6-31G(d) level of theory<sup>34</sup> in a dielectric continuum representing chloroform using the IEF-PCM<sup>31–33</sup> with radii and nonelectrostatic terms for SMD solvation model.<sup>35</sup> Single-point energies in solution including all computed corrections are reported in the text.

**Synthesis of 1a–1g.** The spiroligomers 1a–g, each displaying a benzyl alcohol and a pyridyl or benzyl group, were synthesized as shown in Scheme 1. The synthesis of the diastereomeric bis-amino acids 2a and 2b have been previously described.<sup>11</sup> Each primary amine of 2a and 2b was reductively alkylated with the corresponding benzyl and pyridyl aldehydes 3a–c (Scheme 1 table) with sodium cyanoborohydride at room temperature. The resulting functionalized bis-amino acids were combined with phenyl isocyanate and triethylamine to form phenyl hydantoins. These hydantoins were treated with 33% HBr in acetic acid to remove carboxybenzyl and *tert*-butyl protecting groups to produce amino acids 4a–e after crystallization from methanol. Allyl-carbamate (alloc) protected amino acids 7a–c were synthesized starting from *N*-Boc, *tert*-butyl protected bis-amino acids 5a–c. Each free amine of 5a–c was reductively alkylated with 2-formylbenzyl-allyl-carbonate 6 and sodium cyanoborohydride at room temperature. The resulting functionalized bis-amino acids were exposed to 1-naphthyl isocyanate and triethylamine at room temperature to afford 1-naphthyl hydantoins. Subsequently, Boc and

**Scheme 1. Synthesis of Bifunctional Spiroligomers Together with Their Relative Rate of Acylation by Vinyl Trifluoroacetate**

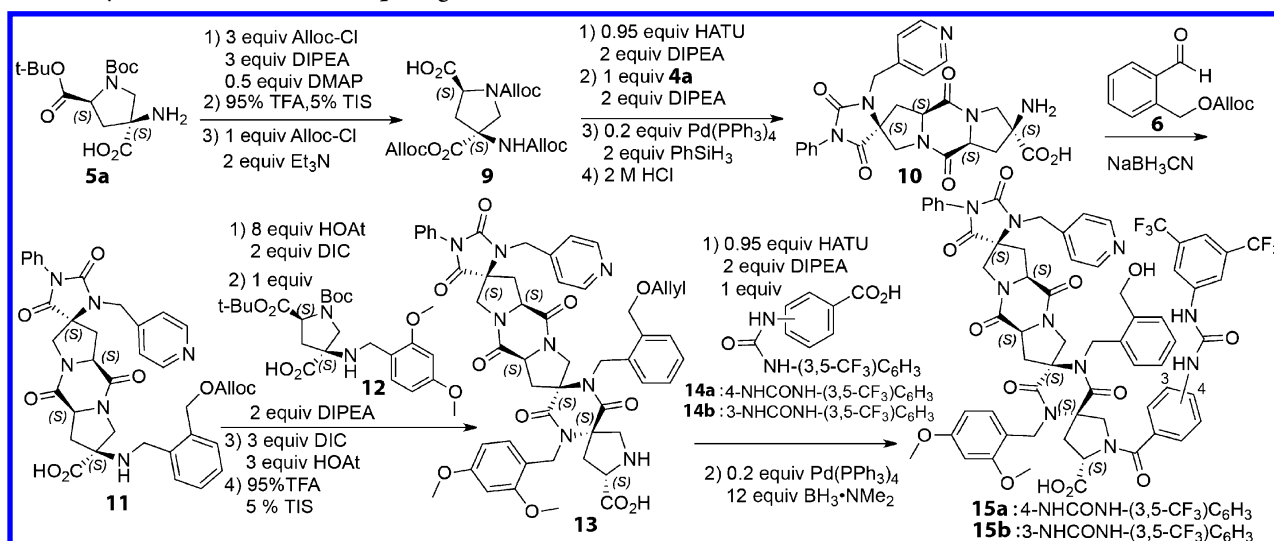


<sup>a</sup>BAA-2, BAA-4, and BAA-7 refer to each of the bis-amino acid monomers 2a–b, 4a–e and 7a–c that were used to construct each compound 1a–g.

*tert*-butyl groups were removed using 95% trifluoroacetic acid (TFA) and 5% tri-isopropylsilane (TIS) as scavengers. Alloc protection of the resulting amino acids using allyl chloroformate and triethylamine produced compounds 7a–c with an overall yield of 65%. The bifunctional spiroligomers 1a–g were synthesized by converting the alloc protected amino acids 7a–c to the 1-hydroxy-7-azabenzotriazole (HOAt) esters and combining them with the amino acids 4a–e together with diisopropylethylamine to form an amide bond. Simultaneous deprotection of the alloc protecting groups and formation of the diketopiperazine by addition of catalytic amount of tetrakis(triphenylphosphine)-palladium(0) with an excess of borane dimethylamine complex as scavenger resulted in compounds 1a–g.

**Synthesis of 15a and 15b.** Synthesis of 15a and 15b was carried out starting from bis-amino acid 5a (Scheme 2). Simultaneous alloc protection of the primary amine and carboxylic acid of 5a was accomplished using allyl chloroformate and DIPEA and DMAP and resulted in the bis-*N*-alloc protected bis-amino acid. Removal of the Boc and *tert*-butyl ester groups was achieved using 95% TFA and 5% TIS. *N*-alloc protection of the resulting amino acid using allyl chloroformate produced compound 9 with an overall yield 95%. Spiroligomer 10 was synthesized by converting alloc protected amino

## Scheme 2. Synthesis of trifunctional spirologomers



acid **9** to the HOAt ester and combining it with the amino acid **4a** together with DIPEA. Quantitative formation of the amide bond was observed over 12 h. Subsequent addition of tetrakis-(triphenylphosphine)palladium(0) and phenylsilane resulted in simultaneous alloc deprotection and diketopiperazine formation within 12 h. Acidic workup with 2 M HCl in ethylacetate gave product **10** with an overall yield of 77% starting from intermediate **9**. Reductive alkylation of amino acid **10** with aldehyde **6** afforded bifunctional amino acid **11**. Trimer **13** was synthesized by converting amino acid **11** to the HOAt ester and combining it with functionalized amino acid **12** together with DIPEA using the acyl transfer reaction that we recently described.<sup>11,54</sup> To promote diketopiperazine formation, an excess of HOAt/DIC was added to the reaction mixture. The crude product was subjected to 95% TFA and 5% TIS to remove the Boc and *tert*-butyl groups. Purification of the mixture produced amino acid **13** in 29% yield from compound **11**. Coupling of the urea benzoic acids bearing bis-amino acids **14a** and **14b** was achieved by preactivation of each of the amino acids with HATU and DIPEA for 10 min and then combining them with the amino acid **11**. The reaction was carried out for 4 h, after which a solution of Pd(PPh<sub>3</sub>)<sub>4</sub> and BH<sub>3</sub>·NMe<sub>2</sub> in dichloromethane was added to the reaction mixture to remove the alloc protecting group and produce trifunctional spirologomers **15a** and **15b** with a 25% yield from **13**.

## RESULTS AND DISCUSSION

We first began by exploring computationally the impact of replacing the carboxylate and imidazole pair of a serine esterase catalytic triad with a simpler pyridine group to investigate how pyridine compares to naturally occurring His-Glu dyads in activating an alcohol as a nucleophile. We generated model transition states (theozymes) to determine the optimal arrangement of the catalytic functional groups for effective catalysis. Two model transition states (Figure 2, **TS1-triad** and **TS1-dyad**) were optimized for the nucleophilic addition of an activated alcohol to vinyl trifluoroacetate using density functional theory.

**TS1-triad** mimics the nucleophilic Ser-His-Glu triad of a typical serine hydrolase active site. The calculations predict a concerted activation/addition mechanism, in which the partially activated oxygen ( $d_{O-H} = 1.21$  Å) attacks the ester ( $d_{C-O} = 2.05$  Å) with an activation free energy of 8.6 kcal/mol with respect to the preorganized catalyst.

**TS1-dyad** features a pyridine-activated alcohol. The nucleophilic addition occurs with a free energy barrier of 14.7

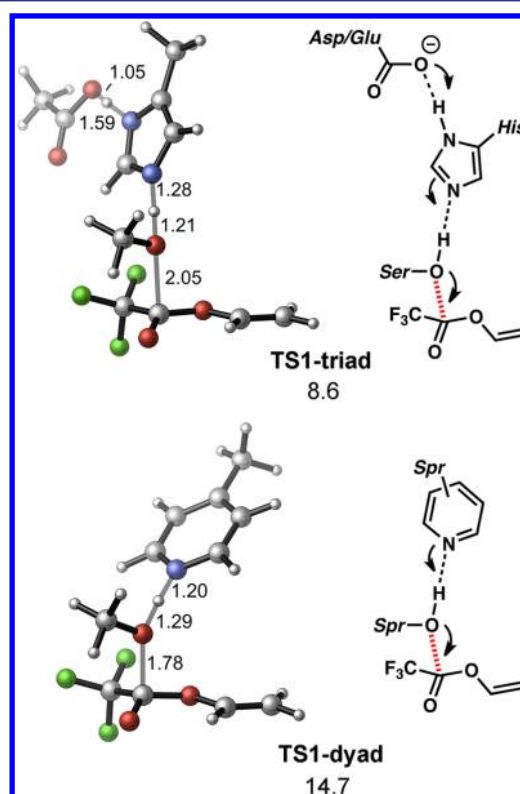


**Figure 2.** Activation of an alcohol as a nucleophile. Transition states [M06-2X/6-31++G(2d,p)(chloroform)//B3LYP/6-31G(d) (chloroform), activation free energies ( $\Delta G^\ddagger$ ) in kcal/mol. Spr: spirologozyme] for the nucleophilic addition of model Ser-His-Asp/Glu triad and pyridine-alcohol dyad to vinyl trifluoroacetate.

kcal/mol, ~6 kcal/mol higher than the barrier for **TS1-triad**. The mechanism is still concerted, but with a late transition state: the forming C–O bond is significantly shorter ( $d_{C-O} = 1.78$  Å), and the proton is closer to pyridine ( $d_{N-H} = 1.20$  Å). In order to investigate the electronic effects of the attachment position of the pyridine to the spirologozyme backbone, we located **TS1-dyad-3pyridyl**, which differs from **TS1-dyad** by the location of the methyl substituent. **TS1-dyad-3pyridyl** and

TS1-dyad are very similar in geometry and in energy (see the SI).

The computed activation free energies with the pyridine–alcohol dyad encouragingly fall in a reasonable range for a catalytic mechanism. However, the relatively high barrier of TS1-dyad compared to that of the triad model suggests that the success of such transformations may be limited to the use of more reactive acyl donors with enhanced electrophilicities. Indeed, vinyl acetate was not consumed in the presence of spiroligozyme **1g** (data not shown), whereas **1g** showed high reactivity relative to benzyl alcohol with vinyl trifluoroacetate.

In order to explore how the nucleophilicity of an alcohol could be enhanced by holding it close to a pyridyl group as a general base, we modeled spiroligomers **1a–g** that would present an alcohol and a pyridyl (**1b–g**) or benzyl (**1a**) pair of functional groups in different relative geometries. Some of the spiroligomers (**1c–g**) could form hydrogen-bonded 18–19 membered rings in order to approximate geometries of the theozyme (TS1-dyad), while others (**1a** and **1b**) would act as control molecules. The modeling suggested that the coupling of the two pro4 bis-amino acids **4a–e** and **7a–c** through a diketopiperazine formed by coupling their proline amino acids could approximate the required geometry.

Kinetic experiments were carried out by combining the spiroligomers **1a–g** with an excess of vinyl trifluoroacetate in CDCl<sub>3</sub> at 22 °C using <sup>19</sup>F NMR (see the SI). Figure 3 shows

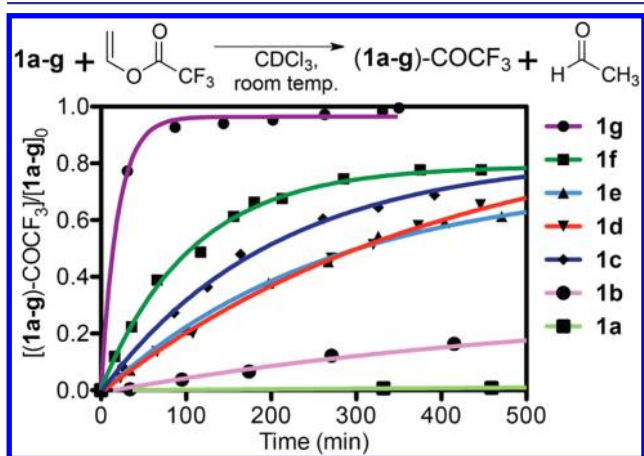


Figure 3. Time-dependent acylation of spiroligomers **1a–g**.

the conversion of spiroligomers to the trifluoroacetate esters over time. These data demonstrate that the stereochemistry of the spiroligomers and the regiochemistry of the pyridyl group tune the relative 3D approach of a pyridyl base to the alcohol, which leads to large differences in activity of the alcohol as a nucleophile. Spiroligomer **1a** is a control molecule that displays a phenyl group instead of a pyridyl group, and the lack of this base results in a very slow rate of acylation; thus, **1a** is defined to have a  $k_{rel}$  of 1 (Scheme 1 table). Spiroligomer **1c** bears a 3-pyridyl group that modeling demonstrates can approach in close proximity to the benzyl alcohol and form a hydrogen bond with it and increase its nucleophilicity; it is acylated 250 times faster than **1a**. Spiroligomers **1d** and **1e** were designed to slightly increase the distance between the 3-pyridyl group and the benzyl alcohol relative to **1c** by altering the relative stereochemistry of stereocenters 1 and 3 to that of stereocenters 2 and 4. Both of these spiroligomers show a slightly slower rate of acylation relative to **1c**. Spiroligomer **1b** holds

the base and the benzyl alcohol on opposite faces of the 5–6–5-fused ring system, and the base cannot form an internal hydrogen bond with the benzyl alcohol. Spiroligomer **1b** becomes acylated slightly faster than **1a**, but its time-dependent acylation data fit better to a kinetic model that was second order in spiroligomer, suggesting that the acylation results from intermolecular activation of the benzyl alcohol by the pyridyl group of a second spiroligomer. Spiroligomer **1g** bears the same stereochemistry as that of **1c** but has a 4-pyridyl group rather than the 3-pyridyl group of **1c**. Compound **1g** is acylated more than 10 times faster than **1c** and exhibits a  $k_{rel}$  value of 2700 over the background reaction. Spiroligomer **1f** was designed to increase the separation between the 4-pyridyl base and the alcohol as in **1e** and was 5-fold slower compared to **1g**.

The relative rate constants of **1a–g** suggest the importance of the correct alignment of the catalytic dyad for effective catalysis. We used molecular dynamics (MD) simulations to study the preorganization of the pyridine and alcohol functionalities in a dynamic environment solvated with chloroform. The results show that the molecules are highly flexible and span a number of alternative conformations (see the SI). The H-bonding interaction of the dyad is disrupted mainly by the favorable interactions of benzyl alcohol with the backbone amide oxygens of the spiroligozyme. MD simulations are indicative of other stable spiroligozyme conformations with substantial deviations from the catalytic arrangement of the dyad. In order to shed light on the effect of structural preferences on reactivity patterns, we performed an extensive conformational analysis of the designed spiroligozymes. We focused our attention on spiroligozymes **1c** and **1g**; their structures differ only by the attachment position of pyridine, but **1g** is acylated ~10-fold faster than **1c**. A high-level quantum mechanical analysis of the conformational space of **1c** and **1g** revealed that the most stable conformers of these spiroligozymes display arrangements that have more buried oxygen nucleophiles and would be expected to be less catalytically active than those with more exposed oxygen nucleophiles. In **1c**, pyridine and benzyl alcohol can form a H-bond in three different orientations (see the SI). The most stable conformer **1c-1** displays an excellent agreement in the arrangement of the catalytic dyad with the QM theozyme (Figure 4a, RMSD = 0.32 Å). However, this orientation unfavorably requires the approach of the ester from the hindered face of the dyad. The conformation that has the most exposed oxygen nucleophile and a pyridine–alcohol hydrogen bond: **1c-2**, lies 2.9 kcal/mol higher in energy than the lowest-energy conformer **1c-1**. The catalytic dyad shows a relatively more distorted arrangement, compared to the ideal geometry of the theozyme (Figure 4a, rmsd = 0.48 Å), but allows the approach of the ester from the less hindered face. As observed in MD simulations, the most stable conformer of **1g**, **1g-1**, shows an alternative favorable interaction, in which benzyl alcohol forms a H-bond with the amide carbonyl of the spiroligozyme rather than with pyridine (Figure 4b, rmsd = 2.10 Å). An analogous conformer of **1c** is also found to be more stable than the reactive conformer **1c-2** (see the SI). Nevertheless, unlike **1c**, the relative positioning of the pyridine and benzyl alcohol in **1g** permits only a single H-bonding conformation for the catalytic dyad: **1g-2**. **1g-2** is 2.3 kcal/mol higher in energy than **1g-1**, and overlays well with the QM theozyme (Figure 4b, rmsd = 0.43 Å).

The results of the MD simulations and conformational analyses show that the designed spiroligozymes present

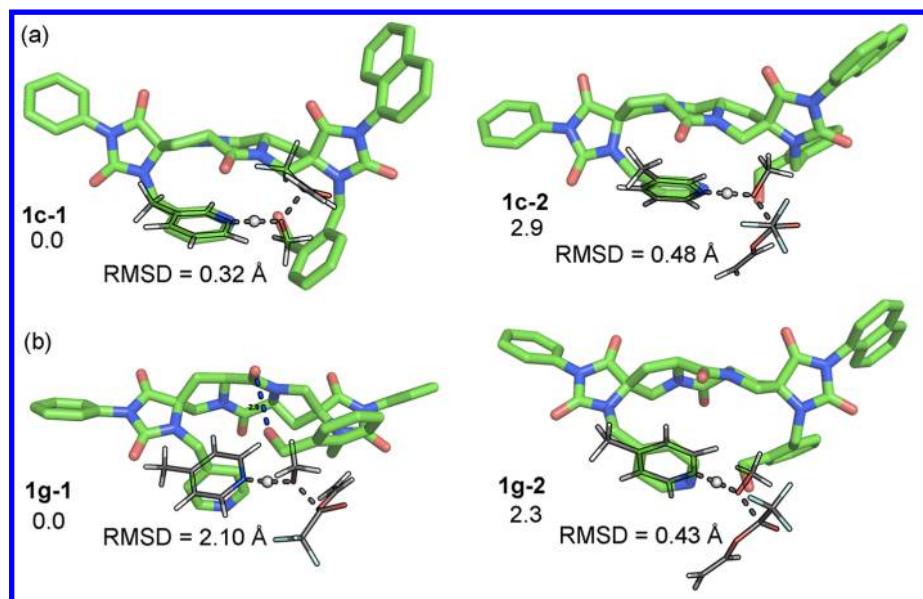


**Figure 4.** Low-energy conformers [M06-2X/6-31G(d) (chloroform), relative electronic energies in kcal/mol with respect to the lowest-energy conformer] of (a) **1c** and (b) **1g** (spiroligozymes, shown in green sticks) overlaid with the corresponding model transition state (theozyme, shown in gray lines).

functional groups in quantum mechanically computed catalytic arrangements, but these functional groups sample multiple conformational states in which a subset is catalytically active. The calculations suggest that eliminating the unproductive conformations of spiroligozymes could significantly enhance the acylation rates. The higher activity of **1g** relative to that of **1c** can be explained, in part, by (1) the lower energetic penalty to adopt a reactive conformation and (2) the closer agreement of the catalytic geometry with the optimal arrangement of the functional groups in the transition state.

Inspired by the rapid formation of acyl–enzyme intermediate in enzyme-catalyzed transesterification reactions, we sought to evaluate spiroligomer **1g** as a catalyst for the transesterification of vinyl trifluoroacetate with methanol. Figure 5 shows the formation of methyl trifluoroacetate over time with 10 mol % of

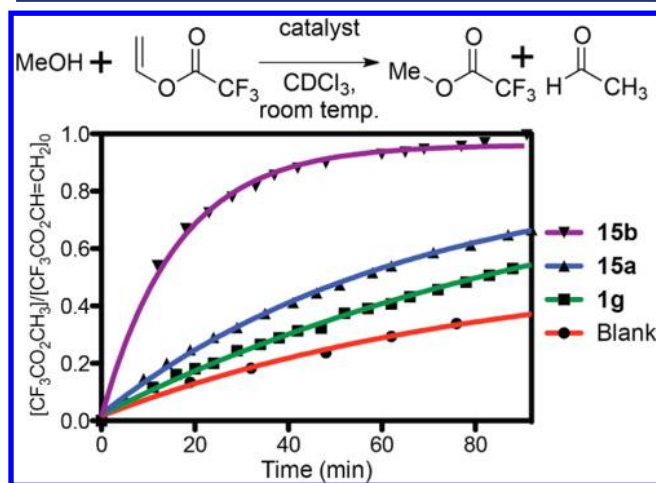


**Figure 5.** A plot of the time-dependent formation of trifluoromethylacetate from trifluorovinylacetate. (Conditions: All reactions are run with 9 mM vinyl trifluoroacetate and 1 mM catalyst. Methanol concentrations: 1.2 M MeOH with **15b**, 1 M MeOH with **15a**, 1.1 M MeOH with **1g**; 1 M MeOH for the blank reaction.)

**1g**. Reactions were carried out under pseudo-first-order conditions with excess methanol. Spiroligomer **1g** shows slightly faster methanolysis than the background reaction of methanol with vinyl trifluoroacetate. The slow formation of product is attributed to the lack of an “oxyanion hole” to stabilize the transition states that follow the formation of the trifluoroacyl–catalyst (**1g**) complex.

In order to improve the rate of acyl transfer from the trifluoroacyl–**1g** intermediate in the second step of transesterification, the trifunctionalized spiroligomers **15a** and **15b** were synthesized. Each bears a urea group as a potential donor of two hydrogen bonds to activate the acyl–spiroligomer intermediate for methanolysis. The modular synthesis of functionalized spiroligomers makes it straightforward to synthesize **15a** and **15b** by extending the synthesis of **1a–g**.

Analysis of the methanolysis reaction of vinyl trifluoroacetate in the presence of 10 mol % trifunctional spiroligomers **15a–15b** demonstrates catalysis of the transesterification reaction. Spiroligomer **15a** bears a 4-substituted urea benzoyl group and shows an acceleration of methanolysis relative to the bifunctional spiroligomer **1g** and the background reaction (Figure 5). Spiroligomer **15b** displays a 3-substituted urea benzoyl and demonstrates an even greater acceleration of transesterification over the background reaction. These results prompted us to calculate second-order rate constants for the **15b**-catalyzed transesterification. The reaction was carried with 6 mol % catalyst under pseudo first-order conditions using 1 M methanol, 0.6 mM **15b**, and different concentration of vinyl trifluoroacetate ranging from 10 mM to 53 mM. Using the steady-state approximation, the rate constants for acylation of compound **15b** ( $k_1$ ) and the subsequent deacylation of the intermediate **15b-Ac** ( $k_2$ ) can be calculated.<sup>10</sup>  $k_{\text{uncat}}$  is measured as the rate of transesterification when methanol is combined with vinyl trifluoroacetate in the absence of base or catalyst. Calculation of second-order rate constants revealed a 2200-fold rate enhancement for  $k_1$  and 130-fold acceleration of  $k_2$ . The resulting ratio of  $k_1$  and  $k_{\text{uncat}}$  is consistent with the  $k_{\text{rel}}$  (2700) observed for the direct acylation of **1g**.

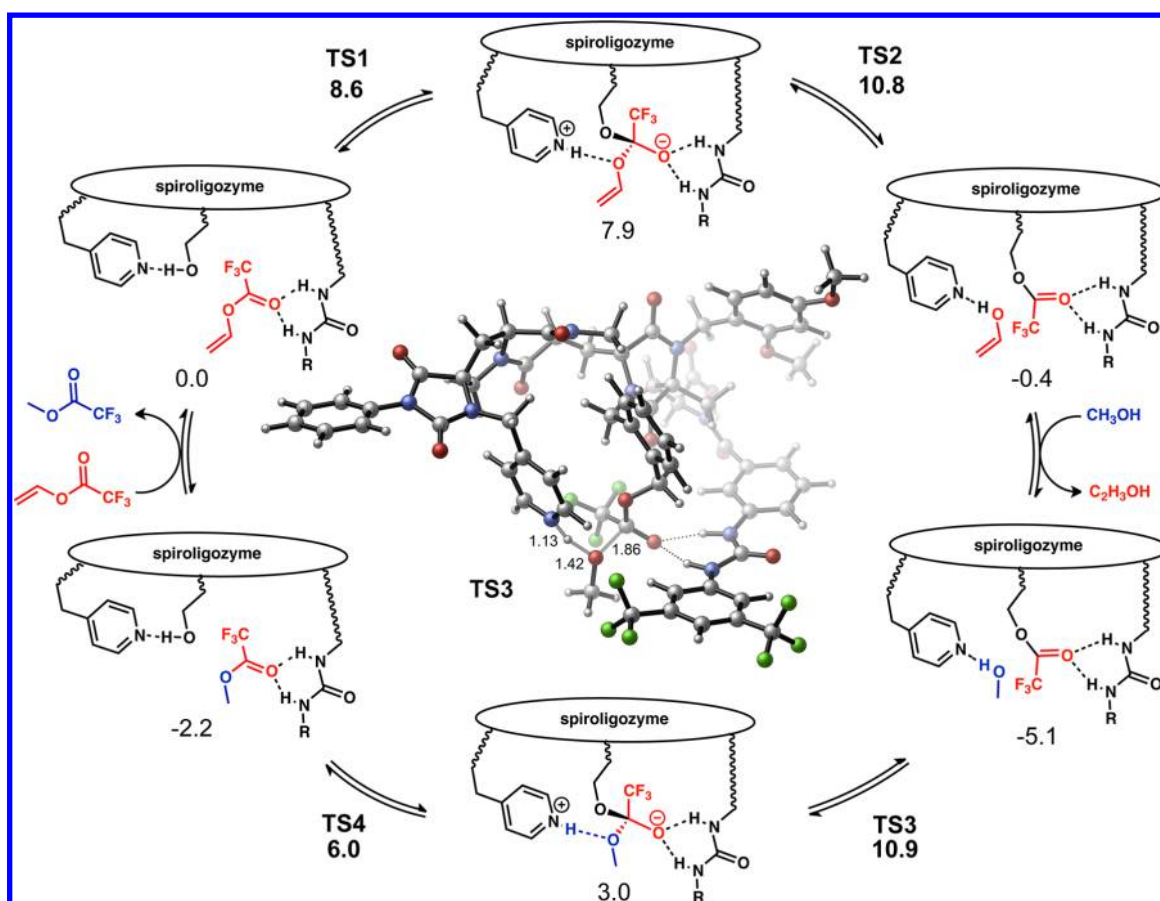


**Figure 6.** Energy profile [M06-2X/6-31G(d)(chloroform)//ONIOM(B3LYP/6-31G(d):PM6); PCM-corrected energies in kcal/mol] for the transesterification of vinyl trifluoroacetate catalyzed by **15b**.

In order to assess whether the newly developed trifunctional spirologozymes function as designed, we calculated the stationary points along the transesterification pathway of vinyl trifluoromethylacetate catalyzed by **15b** (Figure 6, see the SI for 3D representations of all stationary points). The transesterification mechanism involves the pyridine–alcohol dyad that provides the essential nucleophile. Vinyl trifluoroacetate forms a complex with the spirologozyme through H-bonding interactions with the urea. At **TS1**, the benzyl alcohol is partially deprotonated by the general base pyridine, and attacks vinyl trifluoromethylacetate with an activation energy of 8.6 kcal/mol (Figure 6). **TS1** overlays well with the theozyme model involving urea as an oxyanion hole mimic (rmsd = 0.69 Å, see the SI). **TS1** leads to the first tetrahedral intermediate, which is 7.9 kcal/mol higher in energy than the starting complex. The resulting oxyanion is stabilized by the urea, and the protonated pyridine forms an H-bond with the oxygen of the leaving group. This conformational reorganization of pyridine allows general acid-assisted loss of vinyl alcohol (**TS2**) in the next step (Figure 7). **TS2** has an activation barrier of 10.8 kcal/mol and generates the acylated spirologozyme vinyl alcohol complex, which is slightly exothermic by 0.4 kcal/mol. The exchange of vinyl alcohol and methanol leads to an energetically stable acylspirologozyme intermediate, which is 5.1 kcal/mol lower in energy than the starting complex. The reaction then proceeds with the addition of methanol to the acylated spirologozyme via **TS3**. **TS3**, shown in Figure 6, is very similar in geometry to **TS2** (Figure 7). Methanol is partially deprotonated by pyridine; the forming C–O bond is short—

indicative of a late transition state—and the developing negative charge on oxygen is stabilized by the urea. The attack of methanol activated by the general base pyridine is 16.0 kcal/mol uphill from the acyl–spirologozyme intermediate. **TS3** forms the tetrahedral intermediate of the deacylation step, which is 3.0 kcal/mol higher in energy relative to that of the starting complex. Subsequent conformational rearrangement of pyridine leads to **TS4** (Figure 7). Protonated pyridine now acts as a general acid and activates the benzyl alcohol as the leaving group. This promotes the facile cleavage of the covalent bond between the spirologozyme and the substrate ( $\Delta E = 6.0$  kcal/mol), releasing the transesterification product ( $\Delta E = -2.2$  kcal/mol).

The experimental activation free energy of acylation,  $\Delta G^\ddagger_1$ , (**15b**  $k_1 = 0.17 \text{ M}^{-1} \text{ s}^{-1}$ ) is 18.3 kcal/mol, and  $\Delta G^\ddagger_2$  which corresponds to the deacylation step (**15b**  $k_2 = 0.01 \text{ M}^{-1} \text{ s}^{-1}$ ) is 20.0 kcal/mol.<sup>55</sup> The highest calculated barriers for the acylation and deacylation steps are 10.8 and 10.9 kcal/mol respectively (Figure 6, **TS2** and **TS3**). However, these calculated barriers cannot be directly compared to  $\Delta G^\ddagger_1$  and  $\Delta G^\ddagger_2$  because the very large size of the system precludes the calculation of important contributions such as entropies of complex reactant binding, product release, and substrate exchange processes, energetic penalties related to conformational preferences of the species formed in the course of the reaction, and explicit solvent interactions. We estimate the entropy of the complex reactant binding range to be between 4 and 6 kcal/mol,<sup>56</sup> and the conformational energetic penalties are on the order of 3 kcal/mol (see Figure 4). These additional

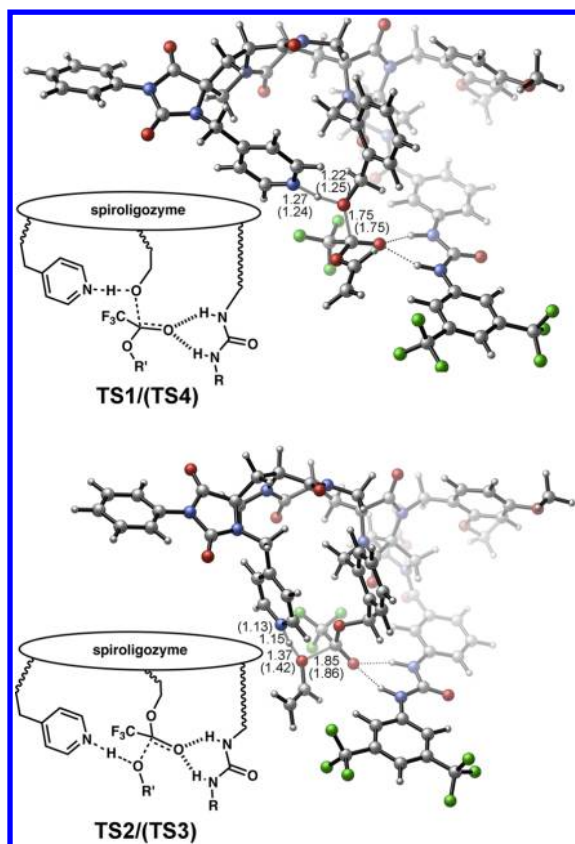


**Figure 7.** Transition structures [Optimized using ONIOM(B3LYP/6-31G(d):PM6). All distances are given in Å. Values in parentheses are the corresponding partial bond distances for TS4 and TS3 ( $R' = \text{CH}_3$ ).] for the transesterification of vinyl trifluoroacetate catalyzed by **15b**.

terms (except for solvent interactions) would positively add to the calculated barriers to bring them in line with the experimental activation free energies,  $\Delta G^\ddagger_1$  and  $\Delta G^\ddagger_2$ .

The optimized intermediates and transition structures clearly demonstrate that the newly developed biomimetic spirologozymes are able to provide correctly positioned catalytic arrays for effective catalysis. Conformational reorganization of catalytic functional groups maintaining optimized TS stabilization along the reaction pathway contributes to catalysis, as described for their natural counterparts.<sup>19</sup> Active sites of natural esterases are also highly preorganized with well-defined and well-maintained interactions in the dynamic environment. However, for di- and trifunctional spirologozymes, avoiding nonproductive conformations through better preorganization of the reactive groups should lead to further lowering of the transition-state energies. As for **1c** and **1g**, the MD simulations for **15b** depict alternative interactions of the catalytic functionalities with the spirologozyme backbone. The most stable conformer of **15b** is 2.4 kcal/mol lower in energy than the reactive conformer (see the SI).

## CONCLUSION

Quantum mechanics and molecular dynamics with empirical force fields have been used to design and analyze a novel type of spirologozyme, a spirocyclic peptidomimetic catalyst with a relative rigid structure that can be designed and synthesized to present functional groups in an arrangement that exhibits multifunctional catalysis. Here, several generations of spiro-

gozymes have been shown to be effective catalysts of methanolysis of the ester, vinyl trifluoroacetate.

## ASSOCIATED CONTENT

### Supporting Information

Computational details, Cartesian coordinates, absolute energies and 3D representations of all optimized structures, snapshots from molecular dynamics simulations, full citation for reference 26, and distance–angle scatter plots for pyridine–alcohol H-bond. This material is available free of charge via the Internet at <http://pubs.acs.org>.

## AUTHOR INFORMATION

### Corresponding Author

meister@temple.edu; houk@chem.ucla.edu

### Notes

The authors declare no competing financial interest.

## ACKNOWLEDGMENTS

This work was supported by the Defense Threat Reduction Agency (DOD-DTRA) (HDTRA1-09-1-0009) and the National Institute of General Medical Sciences, National Institutes of Health (GM36700 and GM067866). We thank the UCLA Institute for Digital Research and Education (IDRE), the Shared Research Computing Services (ShaRCS) Pilot Project for the University of California Systems, and the Extreme Science and Engineering Discovery Environment (XSEDE) for computer time. This research was supported by an allocation of advanced computing resources provided by the National Science Foundation (TG-CHE100059). The computations were performed on Kraken at the National Institute for Computational Sciences (<http://www.nics.tennessee.edu/>). C.E.S. and M.K. thank Dr. Charles DeBrosse for advice and assistance with NMR. We also thank Dr. David Dalton for his insight and helpful discussions.

## REFERENCES

- Radzicka, A.; Wolfenden, R. *Science* **1995**, *267*, 90.
- Zhang, X.; Houk, K. N. *Acc. Chem. Res.* **2005**, *38*, 379.
- Cheong, P. H. Y.; Legault, C. Y.; Um, J. M.; Celebi-Olcum, N.; Houk, K. N. *Chem. Rev.* **2011**, *111*, 5042.
- MacMillan, D. W. C. *Nature* **2008**, *455*, 304.
- Knowles, R. R.; Jacobsen, E. N. *Proc. Natl. Acad. Sci. U.S.A.* **2010**, *107*, 20678.
- Tanaka, F.; Barbas, C. F. *J. Am. Chem. Soc.* **2002**, *124*, 3510.
- Houk, K. N.; Cheong, P. H. Y. *Nature* **2008**, *455*, 309.
- Alberg, D. G.; Poulsen, T. B.; Bertelsen, S.; Christensen, K. L.; Birkler, R. D.; Johannsen, M.; Jorgensen, K. A. *Bioorg. Med. Chem. Lett.* **2009**, *19*, 3888.
- Jarvo, E. R.; Copeland, G. T.; Papaioannou, N.; Bonitatebus, P. J.; Miller, S. J. *J. Am. Chem. Soc.* **1999**, *121*, 11638.
- Ema, T.; Tanida, D.; Matsukawa, T.; Sakai, T. *Chem. Commun.* **2008**, 957.
- Brown, Z. Z.; Schafmeister, C. E. *Org. Lett.* **2010**, *12*, 1436.
- Schafmeister, C. E.; Brown, Z. Z.; Gupta, S. *Acc. Chem. Res.* **2008**, *41*, 1387.
- Zhao, Q.; Lam, Y. H.; Kheirabadi, M.; Xu, C.; Houk, K. N.; Schafmeister, C. E. *J. Org. Chem.* **2012**, *77*, 4784.
- Rothlisberger, D.; Khersonsky, O.; Wollacott, A. M.; Jiang, L.; Dechancie, J.; Betker, J.; Gallaher, J. L.; Althoff, E. A.; Zanghellini, A.; Dym, O.; Albeck, S.; Houk, K. N.; Tawfik, D. S.; Baker, D. *Nature* **2008**, *453*, 190.
- Jiang, L.; Althoff, E. A.; Clemente, F. R.; Doyle, L.; Rothlisberger, D.; Zanghellini, A.; Gallaher, J. L.; Betker, J. L.;

Tanaka, F.; Barbas, C. F.; Hilvert, D.; Houk, K. N.; Stoddard, B. L.; Baker, D. *Science* **2008**, *319*, 1387.

(16) Siegel, J. B.; Zanghellini, A.; Lovick, H. M.; Kiss, G.; Lambert, A. R.; Clair, J. L. S.; Gallaher, J. L.; Hilvert, D.; Gelb, M. H.; Stoddard, B. L.; Houk, K. N.; Michael, F. E.; Baker, D. *Science* **2010**, *329*, 309.

(17) Kirby, A. *Acc. Chem. Res.* **1997**, *30*, 290.

(18) Warshel, A.; Sharma, P. K.; Kato, M.; Xiang, Y.; Liu, H.; Olsson, M. H. M. *Chem. Rev.* **2006**, *106*, 3210.

(19) Smith, A. J. T.; Muller, R.; Toscano, M. D.; Kast, P.; Hellinga, H. W.; Hilvert, D.; Houk, K. N. *J. Am. Chem. Soc.* **2008**, *130*, 15361.

(20) Kiss, G.; Röthlisberger, D.; Baker, D.; Houk, K. N. *Protein Sci.* **2010**, *19*, 1760.

(21) Hedstrom, L. *Chem. Rev.* **2002**, *102*, 4501.

(22) Wright, C. S.; Alden, R. A.; Kraut, J. *Nature* **1969**, *221*, 235.

(23) Schafmeister, C. E. *CANDO*: Computer Aided Nanostructure Design and Optimization software package - under development; 2012.

(24) Richter, F.; Blomberg, R.; Khare, S. D.; Kiss, G.; Kuzin, A. P.; Smith, A. J. T.; Gallaher, J. L.; Pianowski, Z.; Helgenson, R. C.; Grjasnow, A.; Xiao, R.; Seetharam, J.; Su, M.; Vorobev, S.; Lew, S.; Forouhar, F.; Kornhaber, G. J.; Hunt, J. F.; Montelione, G. T.; Tong, L.; Houk, K. N.; Hilvert, D.; Baker, D. *J. Am. Chem. Soc.* **2012**, DOI: 10.1021/ja3037367.

(25) Miller, S. J. *Acc. Chem. Res.* **2004**, *37*, 601.

(26) Frisch, M. J.; et al. *Gaussian 09*, revision C.01; Gaussian, Inc.: Wallingford, CT, 2010; Frisch, M. J.; et al. *Gaussian 03*, revision C.02; Gaussian, Inc.: Wallingford, CT, 2004. See the Supporting Information for the complete reference.

(27) Becke, A. D. *J. Chem. Phys.* **1993**, *98*, 5648.

(28) Lee, C.; Yang, W.; Parr, R. G. *Phys. Rev. B: Condens. Mater. Phys.* **1998**, *37*, 785.

(29) Vosko, S. H.; Wilk, L.; Nusair, M. *Can. J. Phys.* **1980**, *58*, 1200.

(30) Stephens, P. J.; Devlin, F. J.; Chabalowski, C. F.; Frisch, M. J. *J. Phys. Chem.* **1994**, *98*, 11623.

(31) Cossi, M.; Barone, V.; Cammi, R.; Tomasi, J. *Chem. Phys. Lett.* **1996**, *255*, 327.

(32) Cancés, E.; Mennucci, B.; Tomasi, J. *J. Chem. Phys.* **1997**, *107*, 3032.

(33) Tomasi, J.; Mennucci, B.; Cammi, R. *Chem. Rev.* **2005**, *105*, 2999.

(34) Zhao, Y.; Truhlar, D. G. *Theor. Chem. Acc.* **2008**, *120*, 215.

(35) Marenich, A. V.; Cramer, C. J.; Truhlar, D. G. *J. Phys. Chem. B* **2009**, *113*, 6378.

(36) Case, D. A.; Darden, T. A.; Cheatham, I. T. E.; Simmerling, C. L.; Wang, J.; Duke, R. E.; Luo, R.; Walker, R. C.; Zhang, W.; Merz, K. M.; Roberts, B.; Wang, B.; Hayik, S.; Roitberg, A.; Seabra, G.; Kolossváry, I.; Wong, K. F.; Paesani, F.; Vanicek, J.; Liu, J.; Wu, X.; Brozell, S. R.; Steinbrecher, T.; Gohlke, H.; Cai, Q.; Ye, X.; Wang, J.; Hsieh, M. J.; Cui, G.; Roe, D. R.; Mathews, D. H.; Seetin, M. G.; Sagui, C.; Babin, V.; Luchko, T.; Gusarov, S.; Kocalenko, A.; Kollman, P. A. *AMBER 11*; University of California: San Francisco, 2010.

(37) Wang, J.; Wolf, R. M.; Caldwell, J. W.; Kollman, P. A.; Case, D. A. *J. Comput. Chem.* **2004**, *25*, 1157.

(38) Wang, J. M.; Cieplak, P.; Kollman, P. A. *J. Comput. Chem.* **2000**, *21*, 1049.

(39) Bayly, C. I.; Cieplak, P.; Cornell, W. D.; Kollman, P. A. *J. Phys. Chem.* **1993**, *97*, 10269.

(40) Besler, B. H.; Merz, K. M.; Kollman, P. A. *J. Comput. Chem.* **1990**, *11*, 431.

(41) Singh, U. C.; Kollman, P. A. *J. Comput. Chem.* **1984**, *5*, 129.

(42) Cieplak, P.; Caldwell, J. W.; Kollman, P. A. *J. Comput. Chem.* **2001**, *22*, 1048.

(43) Duke, R. E.; Pedersen, L. G. *PMEMD*; University of North Carolina: Chapel Hill; 2003.

(44) Darden, T. A.; York, D.; Pedersen, L. *J. Chem. Phys.* **1993**, *98*, 10089.

(45) Blas, J. R.; Márquez, M.; Sessler, J. L.; Luque, F. J.; Orozco, M. *J. Am. Chem. Soc.* **2002**, *124*, 12796.

(46) *Macromodel* version 9.9; Schrödinger, LLC: New York, NY, 2011.

(47) Banks, J. L.; Beard, H. S.; Cao, Y.; Cho, A. E.; Damm, W.; Farid, R.; Felts, A. K.; Halgren, T. A.; Mainz, D. T.; Maple, J. R.; Murphy, R.; Philipp, D. M.; Repasky, M. P.; Zhang, L. Y.; Berne, B. J.; Friesner, R. A.; Gallicchio, E. *J. Comput. Chem.* **2005**, *26*, 1752.

(48) Polak, E.; Ribiere, G. *Ser. Rouge* **1969**, *16*, 35.

(49) Still, W. C.; Tempczyk, A.; Hawley, R. C.; Hendrickson, T. J. *Am. Chem. Soc.* **1990**, *112*, 6127.

(50) Svensson, M.; Humbel, S.; Morokuma, K. *J. Chem. Phys.* **1996**, *105*, 3654.

(51) Vreven, T.; Morokuma, K. *J. Comput. Chem.* **2000**, *21*, 1419.

(52) Dapprich, S.; Komaromi, I.; Byun, K. S.; Morokuma, K.; Frisch, M. J. *Mol. Struct. (THEOCHEM)* **1999**, *462*, 1.

(53) Stewart, J. J. P. *J. Mol. Model.* **2007**, *13*, 1173.

(54) Brown, Z. Z.; Schafmeister, C. E. *J. Am. Chem. Soc.* **2008**, *130*, 14382.

(55) The experimental activation free energies of acylation and deacylation steps were calculated for **15b** at room temperature using the Eyring–Polanyi equation (see Supporting Information).

(56) Lu, B.; Wong, C. F. *Biopolymers* **2005**, *79*, 277.